

Topological quantum phase transition in an extended Kitaev spin model

Xiao-Feng Shi,^{1,2} Yue Yu,³ J. Q. You,^{1,2} and Franco Nori^{2,4}

¹*Department of Physics and Surface Physics Laboratory (National Key Laboratory), Fudan University, Shanghai 200433, China*

²*Advanced Science Institute, The Institute of Physical and Chemical Research (RIKEN), Wako-shi 351-0198, Japan*

³*Institute of Theoretical Physics, Chinese Academy of Sciences, P.O. Box 2735, Beijing 100190, China*

⁴*Center for Theoretical Physics, Physics Department, Center for the Study of Complex Systems, University of Michigan, Ann Arbor, MI 48109-1040, USA*

(Dated: May 29, 2019)

We study the quantum phase transition between Abelian and non-Abelian phases in an extended Kitaev spin model on the honeycomb lattice, where the periodic boundary condition is applied by placing the lattice on a torus. Our analytical results show that this spin model exhibits a continuous quantum phase transition. Also, we reveal the relationship between bipartite entanglement and the ground-state energy. Our approach directly shows that both the entanglement and the ground-state energy can be used to characterize the topological quantum phase transition in the extended Kitaev model.

I. INTRODUCTION

Quantum phase transitions, which occur when a driving parameter in the Hamiltonian of the system changes across a critical point, play a central role in many important issues in condensed matter physics [1, 2]. While most of the quantum phase transitions can be characterized by symmetry breaking, there is also an exception that can only be witnessed by topological order (see, e.g., [3, 4]). Signatures of topological order in many-body quantum systems can characterize a topological quantum phase transition and include, e.g., the existence of excitations obeying fractional statistics (see, e.g., [5]), ground-state degeneracy related to the topology of the system (instead of the symmetry) (see, e.g., [3, 6]), and topological entanglement entropy [7, 8]. In particular, the spectral Chern number [9] serves as a topological number for characterizing a two-dimensional (2D) system of noninteracting (or weakly interacting) fermions with an energy gap. Without closing the gap, energy spectra with different Chern numbers cannot be deformed into each other [10]. This is because a topological quantum phase transition occurs when changing the Chern number.

Recently, It was shown [11] that the topological quantum phase transition in the Kitaev spin model can be characterized by nonlocal-string order parameters. In an appropriate dual representation, this order parameter can become local and the basic concept of Landau theory of continuous phase transition is also applicable [11].

In the Kitaev model, a $\frac{1}{2}$ -spin is placed at each site of a honeycomb lattice [see Fig. 1(a)] and the interactions between nearest-neighbor spins are highly anisotropic with three types of bonds J_x , J_y , and J_z . To simplify the site-labeling of the honeycomb lattice, one can deform it to a topologically equivalent brick-wall lattice shown in Fig. 1(b). In [11], the topological quantum phase transition of the Kitaev model on a brick-wall lattice is studied using the Hamiltonian below:

$$H_{\text{Kitaev}} = J_x \sum_{n+m=\text{odd}} \sigma_{n,m}^x \sigma_{n+1,m}^x$$

$$+ J_y \sum_{n+m=\text{even}} \sigma_{n,m}^y \sigma_{n+1,m}^y + J_z \sum_{n+m=\text{even}} \sigma_{n,m}^z \sigma_{n,m+1}^z, \quad (1)$$

where $\sigma_{n,m}^x$, $\sigma_{n,m}^y$ and $\sigma_{n,m}^z$ are the Pauli matrices at site (n, m) , with the column index $n = 0, 1, 2, 3, \dots, N-1$ and the row index $m = 0, 1, 2, 3, \dots, M-1$. In [11], the brick-wall lattice is placed on a *cylinder* where the periodic boundary condition is applied in one direction. After exactly solving the model in one vortex-free sector by applying the Jordan-Wigner transformation, a dual transformation is introduced in order to find nonlocal string order parameters for characterizing the topological quantum phase transition. Phase diagrams are shown for systems with widths $M = 1, 2, 4, 6, 8$. For an infinitely large even M , Ref. [11] claims that the gapless region is full of critical lines and that the phase transition from the gapped phase to the gapless phase can be characterized by string order parameters. Note that in order to map an M -row lattice to a $\frac{1}{2}M$ -row lattice, the lattice size should satisfy $N = tM$, where t is an integer.

In the present paper, we study the extended Kitaev model [10, 12] on a honeycomb lattice that is placed on a *torus* (where the periodic boundary condition is applied in two directions) instead of on a cylinder:

$$H = H_{\text{Kitaev}} + J \sum_{n+m=\text{odd}} \sigma_{n,m}^x \sigma_{n+1,m}^z \sigma_{n+2,m}^y + J \sum_{n+m=\text{even}} \sigma_{n,m}^y \sigma_{n+1,m}^z \sigma_{n+2,m}^x. \quad (2)$$

The extended Kitaev model (2) differs from the Kitaev model (1) in that it has a three-spin interaction with magnitude J among every three adjoining sites in each zigzag chain along the x direction. Most importantly, in contrast to the Kitaev model, both Abelian and non-Abelian phases are gapped in the extended model [10]. To use the periodic boundary condition, one needs to have both N and M even; the M th row is equal to the zeroth row and the N th column equal to the zeroth column. Also, the condition $N = tM$ in [11] is not needed.

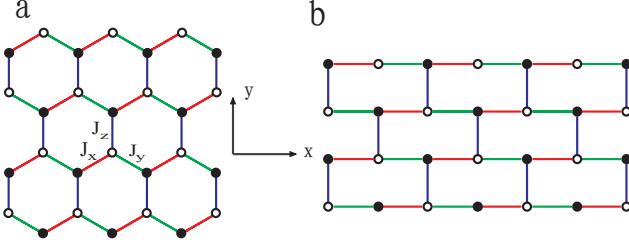


FIG. 1: (Color online) (a) Honeycomb lattice constructed by two triangular lattices that are connected to each other by three types of bonds J_x , J_y and J_z . (b) The brick-wall lattice, which is deformed from the honeycomb lattice in (a). This deformed lattice can be used to label the sites of the honeycomb lattice by column and row indices.

Here we first apply the Jordan-Wigner transformation to the spin operators and then introduce the Majorana fermions to get the ground state of the extended Kitaev model in the vortex-free sector. We show that the third directional derivative of the ground-state energy is discontinuous at each point on the critical line separating the Abelian and non-Abelian phases, while its first and second directional derivatives are continuous at this point. This implies that the topological quantum phase transition is continuous in this extended Kitaev model. Moreover, at this critical point, we also study the non-analyticity of the entanglement (i.e., the von Neumann entropy) between two nearest-neighbor spins and the rest of the spins in the system. We find that the second directional derivative of the von Neumann entropy is closely related to the third directional derivative of the ground-state energy and it is also discontinuous at the critical point. Our approach directly reveals that both the entanglement measure and the ground-state energy can be used to characterize the topological quantum phase transition in the extended Kitaev model.

II. TOPOLOGICAL QUANTUM PHASE TRANSITION

Let us define the Jordan-Wigner transformation [13]

$$\begin{aligned} \sigma_{n,m}^+ &= 2 \left(a_{n,m}^{(s)} \right)^\dagger K(n,m), \\ K(n,m) &= \prod_{n'=0}^{N-1} \prod_{m'=0}^{m-1} \sigma_{n',m'}^z \prod_{n'=1}^{n-1} \sigma_{n',m}^z, \end{aligned} \quad (3)$$

where $s = 1$ if the integer $n + m$ is odd and $s = 2$ if the integer $n + m$ is even. Also, we introduce the following definitions for Majorana fermions:

$$\begin{aligned} i \left[a_{n,m}^{(1)\dagger} - a_{n,m}^{(1)} \right] &= c_{n,m}^{(1)}, \\ a_{n,m}^{(1)\dagger} + a_{n,m}^{(1)} &= d_{n,m}^{(1)} \end{aligned} \quad (4)$$

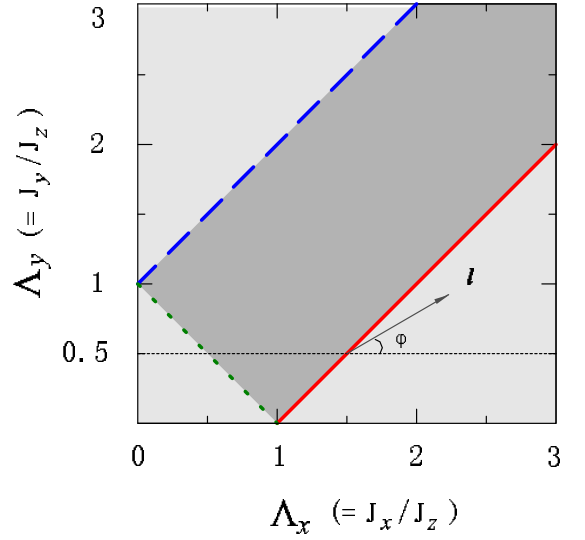


FIG. 2: (Color online) Phase diagram of the extended Kitaev model, where J_x , J_y and $J_z > 0$. The gray region corresponds to the non-Abelian phase and the three triangular (light gray) regions correspond to the Abelian phase. The thick solid, dashed and dotted lines are $\Lambda_x = 1 + \Lambda_y$, $\Lambda_y = 1 + \Lambda_x$, and $\Lambda_y = 1 - \Lambda_x$, where $\Lambda_x \equiv J_x/J_z$ and $\Lambda_y \equiv J_y/J_z$. These lines consist of the boundary of the gray region, which are the critical lines separating the Abelian and non-Abelian phases. The thin dotted line intersects the thick solid and dotted lines at the points $(\Lambda_x, \Lambda_y) = (1.5, 0.5)$ and $(0.5, 0.5)$. The direction l has an inclination angle φ with respect to the horizontal axis and it indicates the direction along which the driving parameters Λ_x and Λ_y vary.

for $n + m$ equal to an odd integer, and

$$\begin{aligned} i \left[a_{n,m}^{(2)\dagger} - a_{n,m}^{(2)} \right] &= d_{n,m}^{(2)}, \\ a_{n,m}^{(2)\dagger} + a_{n,m}^{(2)} &= c_{n,m}^{(2)} \end{aligned} \quad (5)$$

for $n + m$ equal to an even integer. When the phase (arising from the Jordan-Wigner transformation) related to each bond between the $(N - 1)$ th column and the zeroth column is chosen to be $2\pi l$ (l is an integer), the Hamiltonian (2) is reduced to

$$\begin{aligned} H &= iJ_x \sum_{n+m=\text{odd}} c_{n,m}^{(1)} c_{n+1,m}^{(2)} \\ &\quad - iJ_y \sum_{n+m=\text{even}} c_{n,m}^{(2)} c_{n+1,m}^{(1)} \\ &\quad + iJ_z \sum_{n+m=\text{even}} i d_{n,m}^{(2)} d_{n,m+1}^{(1)} c_{n,m}^{(2)} c_{n,m+1}^{(1)} \\ &\quad - iJ \sum_{n+m=\text{odd}} c_{n,m}^{(1)} c_{n+2,m}^{(1)} \\ &\quad + iJ \sum_{n+m=\text{even}} c_{n,m}^{(2)} c_{n+2,m}^{(2)}. \end{aligned} \quad (6)$$

In Eq. (6), the $\frac{1}{2}NM$ operators $i d_{n,m}^{(2)} d_{n,m+1}^{(1)}$, where $n + m$ is an even integer, commute with each other. The

ground state is in the vortex-free sector [12, 14] with $d_{n,m+1}^{(1)} d_{n,m}^{(2)} d_{n+2,m+1}^{(1)} d_{n+2,m}^{(2)} = -1$, which corresponds to the case with the eigenvalue of each plaquette operator [9]

$$W_{(n,m)} = \sigma_{n,m}^x \sigma_{n+1,m}^z \sigma_{n+2,m}^y \sigma_{n,m+1}^y \sigma_{n+1,m+1}^z \sigma_{n+2,m+1}^x \quad (7)$$

equal to 1. Thus, we can set the $\frac{1}{2}NM$ operators $id_{n,m}^{(2)} d_{n,m+1}^{(1)}$ all equal to 1 in Eq. (6), in order to obtain the ground-state energy. For this quadratic Hamiltonian, the Fourier transformation of H via $c_{n,m}^{(1)} = \frac{2}{\sqrt{NM}} \sum_{\mathbf{k}} e^{i\mathbf{k} \cdot \mathbf{r}_{nm}} c_{\mathbf{k}}^{(1)}$ gives rise to

$$H = \sum_{\mathbf{k}} \Phi_{\mathbf{k}}^\dagger H_{\mathbf{k}} \Phi_{\mathbf{k}}, \quad (8)$$

$$H_{\mathbf{k}} = h_x(\mathbf{k}) \sigma^x + h_y(\mathbf{k}) \sigma^y + h_z(\mathbf{k}) \sigma^z,$$

where σ^x, σ^y and σ^z are Pauli matrices, $\Phi_{\mathbf{k}}^\dagger = (c_{-\mathbf{k}}^{(1)}, c_{-\mathbf{k}}^{(2)})$ with $c_{-\mathbf{k}}^{(j)} = (c_{\mathbf{k}}^{(j)})^\dagger$, and

$$h_x(\mathbf{k}) = -J_x \sin\left(\frac{k_x}{2} + \frac{k_y}{2\sqrt{3}}\right) + J_y \sin\left(\frac{k_x}{2} - \frac{k_y}{2\sqrt{3}}\right) - J_z \sin\frac{k_y}{\sqrt{3}},$$

$$h_y(\mathbf{k}) = -J_x \cos\left(\frac{k_x}{2} + \frac{k_y}{2\sqrt{3}}\right) - J_y \cos\left(\frac{k_x}{2} - \frac{k_y}{2\sqrt{3}}\right) + J_z \cos\frac{k_y}{\sqrt{3}},$$

$$h_z(\mathbf{k}) = 2J \sin k_x. \quad (9)$$

Let us define

$$B_{\mathbf{k}} = \frac{\alpha^*(\mathbf{k}) c_{\mathbf{k}}^{(1)} - [\varepsilon(\mathbf{k}) + 2J \sin k_x] c_{\mathbf{k}}^{(2)}}{\sqrt{|\alpha(\mathbf{k})|^2 + [\varepsilon(\mathbf{k}) + 2J \sin k_x]^2}}, \quad (10)$$

where

$$\alpha(\mathbf{k}) = iJ_x e^{i\left(\frac{k_x}{2} + \frac{k_y}{2\sqrt{3}}\right)} + iJ_y e^{-i\left(\frac{k_x}{2} - \frac{k_y}{2\sqrt{3}}\right)} - iJ_z e^{i\frac{k_y}{\sqrt{3}}}, \quad (11)$$

and

$$\varepsilon(\mathbf{k}) = |\mathbf{h}(\mathbf{k})| = \sqrt{|\alpha(\mathbf{k})|^2 + 4J^2 \sin^2 k_x}. \quad (12)$$

It is straightforward to verify that

$$\{B_{\mathbf{k}}^\dagger, B_{\mathbf{k}'}\} = \delta_{\mathbf{k}, \mathbf{k}'}, \quad (13)$$

i.e., $B_{\mathbf{k}}^\dagger$ and $B_{\mathbf{k}}$ are fermionic operators, and the Hamiltonian (8) can be written as

$$H = \sum_{\mathbf{k}} [\varepsilon(\mathbf{k}) - 2\varepsilon(\mathbf{k}) B_{\mathbf{k}}^\dagger B_{\mathbf{k}}]. \quad (14)$$

For Hamiltonian (14), the ground-state energy is $-\sum_{\mathbf{k}} \varepsilon(\mathbf{k})$ and the ground-state $|g\rangle$ obeys $B_{\mathbf{k}}^\dagger B_{\mathbf{k}} |g\rangle = |g\rangle$. The energy spectrum $\varepsilon(\mathbf{k})$ is *gapless* [10] only when $J_x = J_y + J_z$, or $J_y = J_z + J_x$, or $J_z = J_x + J_y$, which corresponds to the thick solid, dashed, and dotted lines in Fig. 2, respectively.

When $J > 0$, the spectral Chern number is 1 if $J_x < J_y + J_z, J_y < J_z + J_x$ and $J_z < J_x + J_y$, and 0 if $J_x > J_y + J_z$ or $J_y > J_z + J_x$ or $J_z > J_x + J_y$ (see [9, 10]). These two cases correspond to the non-Abelian and Abelian phases in the extended Kitaev model and both of them are *gapped* topological phases. The phase diagram is shown in Fig. 2, where the gray area corresponds to the non-Abelian phase and the critical lines (denoted as thick solid, dashed and dotted lines) separate the Abelian and non-Abelian phases. This indicates that the system can experience quantum phase transitions across these three thick lines. Here we rescale the inter-spin coupling strengths by introducing $\Lambda_x \equiv J_x/J_z, \Lambda_y \equiv J_y/J_z$, and $\Lambda \equiv J/J_z$, so as to conveniently characterize the quantum phase transition.

To demonstrate the quantum phase transition, one may reveal the nonanalyticity of the ground-state energy. The ground-state energy per site is

$$E = -\frac{1}{NM} \sum_{\mathbf{k}} \varepsilon(\mathbf{k}) = -\frac{\sqrt{3}}{16\pi^2} \int_{\text{BZ}} d^2k \varepsilon(\mathbf{k}), \quad (15)$$

where BZ denotes the first Brillouin zone. Its directional derivatives with respect to the driving parameter along any given direction \mathbf{l} (see Fig. 2) are

$$\begin{aligned} \frac{\partial E}{\partial l} &= \cos \varphi \frac{\partial E}{\partial \Lambda_x} + \sin \varphi \frac{\partial E}{\partial \Lambda_y}, \\ \frac{\partial^2 E}{\partial l^2} &= \cos^2 \varphi \frac{\partial^2 E}{\partial \Lambda_x^2} + \sin 2\varphi \frac{\partial^2 E}{\partial \Lambda_x \partial \Lambda_y} + \sin^2 \varphi \frac{\partial^2 E}{\partial \Lambda_y^2}, \\ \frac{\partial^3 E}{\partial l^3} &= \cos^3 \varphi \frac{\partial^3 E}{\partial \Lambda_x^3} + 3 \sin \varphi \cos^2 \varphi \frac{\partial^3 E}{\partial \Lambda_y \partial \Lambda_x^2} \\ &\quad + 3 \sin^2 \varphi \cos \varphi \frac{\partial^3 E}{\partial \Lambda_x \partial \Lambda_y^2} + \sin^3 \varphi \frac{\partial^3 E}{\partial \Lambda_y^3}, \\ &\dots \dots \dots \end{aligned} \quad (16)$$

If the n th directional derivative $\partial^n E / \partial l^n$ ($n=1, 2, \dots$) is nonanalytical at the critical point $(\Lambda_x^c, \Lambda_y^c)$, and the directional derivatives $\partial^m E / \partial l^m$ with $0 \leq m < n$ are analytical there, a topological quantum phase transition occurs at this critical point.

It can be proved that (see Appendix A)

$$\begin{aligned} \left. \frac{\partial E}{\partial l} \right|_{1+} &= \left. \frac{\partial E}{\partial l} \right|_{1-}, \\ \left. \frac{\partial^2 E}{\partial l^2} \right|_{1+} &= \left. \frac{\partial^2 E}{\partial l^2} \right|_{1-}, \end{aligned} \quad (17)$$

and

$$\left. \frac{\partial^3 E}{\partial l^3} \right|_{1+} - \left. \frac{\partial^3 E}{\partial l^3} \right|_{1-} \simeq \frac{\sqrt{6} \mathcal{D}^3}{2\pi^2} \Gamma, \quad (18)$$

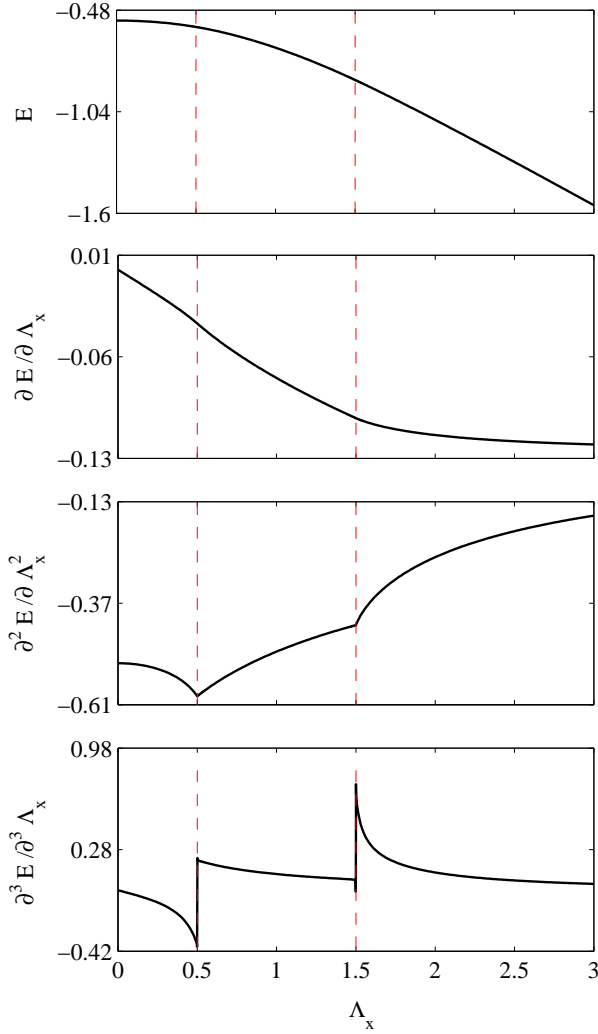


FIG. 3: The ground-state energy per site E (in units of J_z) and its first, second, and third derivatives with respect to Λ_x , where $\Lambda_y = 0.5$, $\Lambda = 0.1$ and $\varphi = 0$ (which corresponds to the horizontal thin dotted line in Fig. 2). It is clear that E and $\partial E/\partial \Lambda_x$ are continuous functions, but $\partial^3 E/\partial \Lambda_x^3$ is discontinuous at the transition points $\Lambda_x = 0.5$ and 1.5 .

where

$$\mathcal{D} = \cos\left(\varphi + \frac{\pi}{4}\right),$$

$$\Gamma = \int_0^{2\pi} d\theta \frac{1}{Q_1 + Q_2 \sin(2\theta + \phi_1)}, \quad (19)$$

1^+ denotes $(\Lambda_x - \Lambda_y) \rightarrow 1$ with $(\Lambda_x - \Lambda_y) > 1$, and 1^- denotes $(\Lambda_x - \Lambda_y) \rightarrow 1$ with $(\Lambda_x - \Lambda_y) < 1$. In (19),

$$Q_1 = \frac{1}{2}(4\Lambda^2 + \Lambda_y^2 + \Lambda_y + 1),$$

$$Q_2 = \frac{1}{4}\sqrt{(8\Lambda^2 + 2\Lambda_y^2 + 2\Lambda_y - 1)^2 + 3(1 + 2\Lambda_y)^2},$$

$$\phi_1 = \arctan \frac{8\Lambda^2 + 2\Lambda_y^2 + 2\Lambda_y - 1}{\sqrt{3}(1 + 2\Lambda_y)}. \quad (20)$$

Equations (17) and (18) reveal that a continuous topological quantum phase transition occurs across the critical line $\Lambda_x = 1 + \Lambda_y$ (denoted by the thick solid line in Fig. 2). Similarly, it can be shown that such a continuous topological quantum phase transition also occurs across the critical lines $\Lambda_y = 1 + \Lambda_x$ and $\Lambda_x = 1 - \Lambda_y$ (denoted, respectively, by the thick dashed and dotted lines in Fig. 2). As a numerical test, we choose $\Lambda = 0.1$, $\varphi = 0$ and $\Lambda_y = 0.5$ to show this quantum phase transition in Fig. 3, where the range of Λ_x is chosen by the thin dotted line in Fig. 2. It can be seen in Fig. 3 that the ground-state energy and its first and second directional derivatives are continuous for each Λ_x , while its third directional derivative is nonanalytic at the points $\Lambda_x = 0.5$ and $\Lambda_x = 1.5$. These two points satisfy the condition $J_z = J_x + J_y$ and $J_x = J_y + J_z$, respectively. It is obvious that these two points are on the critical lines denoted by the thick dotted and solid lines in Fig. 2.

III. ENTANGLEMENT

It has been shown that the entanglement also exhibits critical behavior at the quantum phase transition point for both spin (see, e.g., [16, 17, 18]) and fermionic systems (see, e.g., [19, 20]). Also, it was shown [21, 22] that there is a general relation between the bipartite entanglement and the quantum phase transition. In this section, we show that the nonanalyticity of the ground-state energy in the extended Kitaev model results from the correlation functions [see Eqs. (24), (28) and (29) for their definitions]. Furthermore, we show that the bipartite entanglement also exhibits nonanalyticity at the quantum phase transition point and its nonanalyticity is also due to the nonanalyticity of the same correlation functions. This reveals that both the ground-state energy and the bipartite entanglement can characterize the quantum phase transition in the extended Kitaev model.

A. Correlation functions and nonanalyticity of ground-state energy

From Hellmann-Feynman theorem [23], we have

$$\frac{\partial E}{\partial l} = \frac{1}{NM} \text{Tr} \left(\rho \frac{\partial H}{\partial l} \right)$$

$$= \frac{1}{NM} \cos \varphi \sum_{n+m=\text{odd}} \text{Tr} (\rho \sigma_{n,m}^x \sigma_{n+1,m}^x)$$

$$+ \frac{1}{NM} \sin \varphi \sum_{n+m=\text{even}} \text{Tr} (\rho \sigma_{n,m}^y \sigma_{n+1,m}^y), \quad (21)$$

where E is the ground-state energy per site given in Eq. (15), H is the Hamiltonian (2) (rescaled by J_z), Tr denotes the trace over the ground-state subspace, and $\rho = |g\rangle\langle g|$ is the density matrix of the system. When $|g\rangle\langle g|$ is traced over all spins except the two spins at $\mathbf{r}_{n,m}$

and $\mathbf{r}_{n',m'}$, the reduced density matrix is

$$\begin{aligned}\rho(\mathbf{r}_{n,m}, \mathbf{r}_{n',m'}) &= \text{Tr}'(|g\rangle\langle g|) \\ &= \frac{1}{4} \sum_{\alpha, \alpha'=0}^3 \langle g | \sigma_{n,m}^\alpha \sigma_{n',m'}^{\alpha'} | g \rangle \\ &\quad \times \sigma_{n,m}^\alpha \sigma_{n',m'}^{\alpha'},\end{aligned}\quad (22)$$

where $\sigma^\alpha (\sigma^{\alpha'})$ are Pauli matrices σ^x, σ^y and σ^z for $\alpha (\alpha')=1$ to 3, and the unit matrix for $\alpha (\alpha')=0$. When the two spins at $\mathbf{r}_{n,m}$ and $\mathbf{r}_{n+1,m}$ are linked by an x -type bond, the reduced density matrix becomes

$$\begin{aligned}\rho(\mathbf{r}_{n,m}, \mathbf{r}_{n+1,m}) &= \frac{1}{4} \langle g | \sigma_{n,m}^x \sigma_{n+1,m}^x | g \rangle \sigma_{n,m}^x \sigma_{n+1,m}^x \\ &\quad + \frac{1}{4} I_{n,m} I_{n+1,m}\end{aligned}\quad (23)$$

where $n+m$ is an odd integer, and I is the unit operator.

Because of translational invariance, the correlation function

$$\mathcal{G}_x \equiv \langle g | \sigma_{n,m}^x \sigma_{n+1,m}^x | g \rangle \quad (24)$$

is spatially invariant. Thus, Eq. (23) can be written as

$$\rho(\mathbf{r}_{n,m}, \mathbf{r}_{n+1,m}) = \frac{I_{n,m} I_{n+1,m} + \mathcal{G}_x \sigma_{n,m}^x \sigma_{n+1,m}^x}{4}, \quad (25)$$

where $n+m$ is an odd integer. Similarly, one has

$$\rho(\mathbf{r}_{n,m}, \mathbf{r}_{n+1,m}) = \frac{I_{n,m} I_{n+1,m} + \mathcal{G}_y \sigma_{n,m}^y \sigma_{n+1,m}^y}{4}, \quad (26)$$

$$\rho(\mathbf{r}_{n,m}, \mathbf{r}_{n,m+1}) = \frac{I_{n,m} I_{n,m+1} + \mathcal{G}_z \sigma_{n,m}^z \sigma_{n,m+1}^z}{4}, \quad (27)$$

with

$$\mathcal{G}_y \equiv \langle g | \sigma_{n,m}^y \sigma_{n+1,m}^y | g \rangle, \quad (28)$$

$$\mathcal{G}_z \equiv \langle g | \sigma_{n,m}^z \sigma_{n,m+1}^z | g \rangle, \quad (29)$$

where $n+m$ is an even integer for both \mathcal{G}_y and \mathcal{G}_z . Here Eqs. (25)-(27) are the results obtained for the reduced density matrix when the two spins at $\mathbf{r}_{n,m}$ and $\mathbf{r}_{n',m'}$ are nearest-neighbors. When the two spins at $\mathbf{r}_{n,m}$ and $\mathbf{r}_{n',m'}$ are not nearest-neighbors, the density matrix is

$$\rho(\mathbf{r}_{n,m}, \mathbf{r}_{n',m'}) = \frac{I_{n,m} I_{n',m'}}{4}. \quad (30)$$

Using the Jordan-Wigner transformation (3) and the definitions (4) and (5) for the Majorana fermions, we can derive that

$$\mathcal{G}_x = \langle g | \sigma_{0,1}^x \sigma_{1,1}^x | g \rangle = i \langle g | c_{0,1}^{(1)} c_{1,1}^{(2)} | g \rangle. \quad (31)$$

From Eqs. (10), (12), and (31) we have

$$\begin{aligned}\mathcal{G}_x &= \frac{\sqrt{3}i}{8\pi^2} \int_{\text{BZ}} d^2k \frac{\alpha(\mathbf{k})}{\varepsilon(\mathbf{k})} \exp\left(-i\frac{k_x}{2} - i\frac{\sqrt{3}k_y}{6}\right) \\ &= \frac{-\sqrt{3}}{8\pi^2} \int_{\text{BZ}} d^2k \frac{1}{\sqrt{|\alpha(\mathbf{k})|^2 + 4\Lambda^2 \sin^2 k_x}} \\ &\quad \times \left[\Lambda_x + \Lambda_y \cos k_x - \cos \frac{k_x + \sqrt{3}k_y}{2} \right],\end{aligned}\quad (32)$$

and

$$\begin{aligned}|\mathcal{G}_x| &\leq \frac{\sqrt{3}}{8\pi^2} \int_{\text{BZ}} d^2k \frac{|\alpha(\mathbf{k})|}{\varepsilon(\mathbf{k})} \\ &< \frac{\sqrt{3}}{8\pi^2} \int_{\text{BZ}} d^2k \frac{\varepsilon(\mathbf{k})}{\varepsilon(\mathbf{k})} = 1,\end{aligned}\quad (33)$$

which gives rise to $-1 < \mathcal{G}_x < 1$. Similarly, we have

$$\begin{aligned}\mathcal{G}_y &= \frac{-\sqrt{3}}{8\pi^2} \int_{\text{BZ}} d^2k \frac{1}{\sqrt{|\alpha(\mathbf{k})|^2 + 4\Lambda^2 \sin^2 k_x}} \\ &\quad \times \left[\Lambda_x \cos k_x + \Lambda_y - \cos \frac{k_x - \sqrt{3}k_y}{2} \right],\end{aligned}\quad (34)$$

with $-1 < \mathcal{G}_y < 1$.

From Eqs. (21), (24), and (28), it follows that

$$\begin{aligned}\frac{\partial E}{\partial l} &= \frac{1}{2} \cos \varphi \mathcal{G}_x + \frac{1}{2} \sin \varphi \mathcal{G}_y, \\ \frac{\partial^2 E}{\partial l^2} &= \frac{1}{2} \cos^2 \varphi \frac{\partial \mathcal{G}_x}{\partial \Lambda_x} + \frac{1}{2} \sin^2 \varphi \frac{\partial \mathcal{G}_y}{\partial \Lambda_y} \\ &\quad + \frac{1}{2} \sin \varphi \cos \varphi \left[\frac{\partial \mathcal{G}_x}{\partial \Lambda_y} + \frac{\partial \mathcal{G}_y}{\partial \Lambda_x} \right], \\ \frac{\partial^3 E}{\partial l^3} &= \frac{1}{2} \cos^3 \varphi \frac{\partial^2 \mathcal{G}_x}{\partial \Lambda_x^2} + \frac{1}{2} \sin^3 \varphi \frac{\partial^2 \mathcal{G}_y}{\partial \Lambda_y^2} \\ &\quad + \frac{1}{2} \cos^2 \varphi \sin \varphi \left[2 \frac{\partial^2 \mathcal{G}_x}{\partial \Lambda_x \partial \Lambda_y} + \frac{\partial^2 \mathcal{G}_y}{\partial \Lambda_x^2} \right] \\ &\quad + \frac{1}{2} \cos \varphi \sin^2 \varphi \left[2 \frac{\partial^2 \mathcal{G}_y}{\partial \Lambda_x \partial \Lambda_y} + \frac{\partial^2 \mathcal{G}_x}{\partial \Lambda_y^2} \right].\end{aligned}\quad (35)$$

Equation (35) shows that the directional derivatives of the ground-state energy per site are determined by the correlation functions \mathcal{G}_α ($\alpha = x, y$) and their derivatives. Section II shows that $\partial E / \partial l$ and $\partial^2 E / \partial l^2$ are continuous, while $\partial^3 E / \partial l^3$ is *discontinuous* on the critical line, e.g., $\Lambda_x = 1 + \Lambda_y$ (i.e., the thick solid line in Fig. 2). Equation (35) reveals that the nonanalyticity of E on the critical line is due to the nonanalyticity of \mathcal{G}_α . As shown in Appendix B,

$$\begin{aligned}\mathcal{G}_\alpha|_{1+} &= \mathcal{G}_\beta|_{1-}, \\ \frac{\partial \mathcal{G}_\alpha}{\partial \Lambda_\beta}|_{1+} &= \frac{\partial \mathcal{G}_\alpha}{\partial \Lambda_\beta}|_{1-},\end{aligned}\quad (36)$$

where $\alpha, \beta = x, y$, and

$$\begin{aligned}\frac{\partial^2 \mathcal{G}_x}{\partial \Lambda_x^2}|_{1+} - \frac{\partial^2 \mathcal{G}_x}{\partial \Lambda_x^2}|_{1-} &\simeq \frac{\sqrt{3}}{2\pi^2} \Gamma, \\ \frac{\partial^2 \mathcal{G}_x}{\partial \Lambda_x \partial \Lambda_y}|_{1+} - \frac{\partial^2 \mathcal{G}_x}{\partial \Lambda_x \partial \Lambda_y}|_{1-} &\simeq -\frac{\sqrt{3}}{2\pi^2} \Gamma, \\ \frac{\partial^2 \mathcal{G}_x}{\partial \Lambda_y^2}|_{1+} - \frac{\partial^2 \mathcal{G}_x}{\partial \Lambda_y^2}|_{1-} &\simeq \frac{\sqrt{3}}{2\pi^2} \Gamma, \\ \frac{\partial^2 \mathcal{G}_y}{\partial \Lambda_x^2}|_{1+} - \frac{\partial^2 \mathcal{G}_y}{\partial \Lambda_x^2}|_{1-} &\simeq -\frac{\sqrt{3}}{2\pi^2} \Gamma,\end{aligned}$$

$$\left. \frac{\partial^2 \mathcal{G}_y}{\partial \Lambda_x \partial \Lambda_y} \right|_{1+} - \left. \frac{\partial^2 \mathcal{G}_y}{\partial \Lambda_x \partial \Lambda_y} \right|_{1-} \simeq \frac{\sqrt{3}}{2\pi^2} \Gamma,$$

$$\left. \frac{\partial^2 \mathcal{G}_y}{\partial \Lambda_y^2} \right|_{1+} - \left. \frac{\partial^2 \mathcal{G}_y}{\partial \Lambda_y^2} \right|_{1-} \simeq -\frac{\sqrt{3}}{2\pi^2} \Gamma,$$

where Γ is given in Eq. (19). Equation (37) shows the spin-spin correlation function \mathcal{G}_α can signal the quantum phase transition, similar to the bond-bond correlation function in the Kitaev model [15]. From Eqs and (37), we have

$$\left. \frac{\partial^3 E}{\partial l^3} \right|_{1+} - \left. \frac{\partial^3 E}{\partial l^3} \right|_{1-} \simeq \frac{\sqrt{3}(\cos \varphi - \sin \varphi)^3}{4\pi^2} \Gamma = \frac{\sqrt{6}\epsilon}{2\pi}$$

which is the same as in Eq. (18). This further reveals that the nonanalyticity of the ground-state energy is from the nonanalyticity of the correlation function.

B. Nonanalyticity of entanglement

We focus on the bipartite entanglement of the ground state $|g\rangle$ between two spins (at $\mathbf{r}_{n,m}$ and $\mathbf{r}_{n',m'}$) and the rest of the spins in the system. We use the von Neumann entropy to measure the entanglement between these two spins and the rest of the spins in the system. The von Neumann entropy can be defined by [24]

$$S_\alpha = -\text{Tr}[\rho(\mathbf{r}_{n,m}, \mathbf{r}_{n+1,m}) \log_2 \rho(\mathbf{r}_{n,m}, \mathbf{r}_{n+1,m})], \quad (39)$$

where Tr denotes the trace over the two-spin Hilbert space, and $\alpha = x$ if $n + m$ is an odd integer, and $\alpha = y$ if $n + m$ is an even integer. Also, this entropy can be written as

$$S_\alpha = -\sum \lambda_i \log_2 \lambda_i, \quad (40)$$

where the sum runs over the four eigenvalues λ_i of the matrix $\rho(\mathbf{r}_{n,m}, \mathbf{r}_{n+1,m})$. From Eqs. (24) and (28), it follows that

$$\lambda_1 = \lambda_2 = \frac{1}{4}(1 + \mathcal{G}_\alpha),$$

$$\lambda_3 = \lambda_4 = \frac{1}{4}(1 - \mathcal{G}_\alpha). \quad (41)$$

Thus, we have the entanglement measure

$$S_\alpha = 2 - \frac{1}{2} \log_2 [(1 - \mathcal{G}_\alpha)^{1-\mathcal{G}_\alpha} (1 + \mathcal{G}_\alpha)^{1+\mathcal{G}_\alpha}], \quad (42)$$

which is determined by the correlation function \mathcal{G}_α , similar to the thermal entanglement [25].

To see the relationship between the entanglement and the quantum phase transition, we analyze the directional derivatives of the von Neumann entropy with respect to the driving parameters along any direction \mathbf{l} . The first

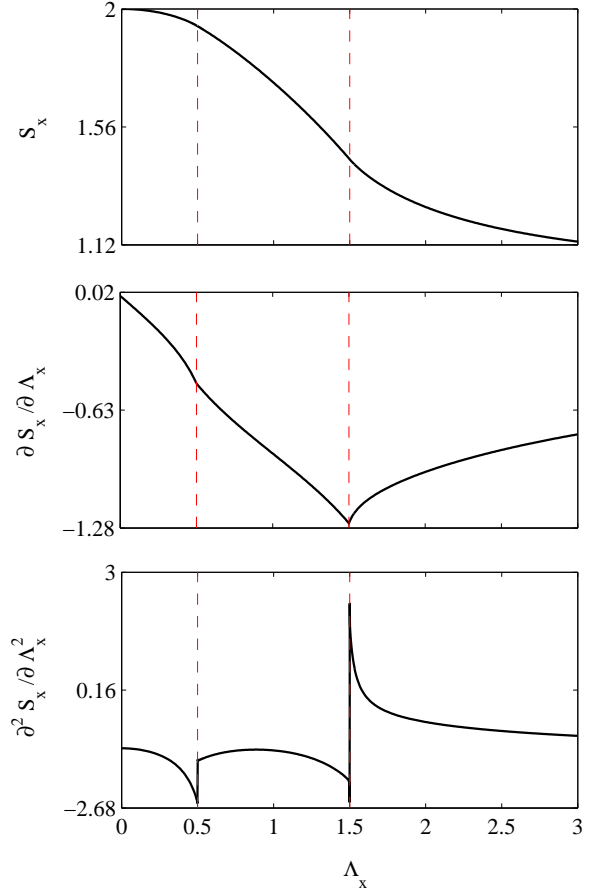


FIG. 4: The bipartite entanglement (i.e., the von Neumann entropy) S_x and its first, and second derivatives with respect to Λ_x , where $\Lambda_y = 0.5$, $\Lambda = 0.1$ and $\varphi = 0$ (which corresponds to the horizontal thin dotted line in Fig. 2). Obviously, S_x and $\partial S_x / \partial \Lambda_x$ are continuous functions, but $\partial^2 S_x / \partial \Lambda_x^2$ is discontinuous at the transition points $\Lambda_x = 0.5$ and 1.5 .

and second directional derivatives of the bipartite entanglement are

$$\frac{\partial S_\alpha}{\partial l} = \frac{\partial \mathcal{G}_\alpha}{\partial l} \log_2 \sqrt{\frac{1 - \mathcal{G}_\alpha}{1 + \mathcal{G}_\alpha}},$$

$$\frac{\partial^2 S_\alpha}{\partial l^2} = \frac{\partial^2 \mathcal{G}_\alpha}{\partial l^2} \log_2 \sqrt{\frac{1 - \mathcal{G}_\alpha}{1 + \mathcal{G}_\alpha}} - \frac{1}{\ln 2} \frac{\partial \mathcal{G}_\alpha}{\partial l} \frac{1}{1 - \mathcal{G}_\alpha^2}. \quad (43)$$

where

$$\frac{\partial \mathcal{G}_\alpha}{\partial l} = \cos \varphi \frac{\partial \mathcal{G}_\alpha}{\partial \Lambda_x} + \sin \varphi \frac{\partial \mathcal{G}_\alpha}{\partial \Lambda_y},$$

$$\frac{\partial^2 \mathcal{G}_\alpha}{\partial l^2} = \cos^2 \varphi \frac{\partial^2 \mathcal{G}_\alpha}{\partial \Lambda_x^2} + \sin 2\varphi \frac{\partial^2 \mathcal{G}_\alpha}{\partial \Lambda_x \partial \Lambda_y} + \sin^2 \varphi \frac{\partial^2 \mathcal{G}_\alpha}{\partial \Lambda_y^2}. \quad (44)$$

From Eqs. (36), (37), (42), and (43), we have

$$S_\alpha|_{1+} = S_\alpha|_{1-},$$

$$\left. \frac{\partial S_\alpha}{\partial l} \right|_{1+} = \left. \frac{\partial S_\alpha}{\partial l} \right|_{1-}, \quad (45)$$

and

$$\begin{aligned} \frac{\partial^2 S_x}{\partial l^2} \Big|_{1+} - \frac{\partial^2 S_x}{\partial l^2} \Big|_{1-} &\simeq \frac{\sqrt{3}\Gamma\mathcal{D}^2}{\pi^2} \log_2 \sqrt{\frac{1-\mathcal{G}_x^c}{1+\mathcal{G}_x^c}}, \\ \frac{\partial^2 S_y}{\partial l^2} \Big|_{1+} - \frac{\partial^2 S_y}{\partial l^2} \Big|_{1-} &\simeq -\frac{\sqrt{3}\Gamma\mathcal{D}^2}{\pi^2} \log_2 \sqrt{\frac{1-\mathcal{G}_y^c}{1+\mathcal{G}_y^c}}, \end{aligned} \quad (46)$$

where

$$\mathcal{G}_\alpha^c = \mathcal{G}_\alpha|_{1+} = \mathcal{G}_\alpha|_{1-}. \quad (47)$$

Equation (46) shows that the bipartite entanglement is nonanalytic with its second directional derivative $\partial^2 S_\alpha / \partial l^2$ discontinuous at the critical line $\Lambda_x = 1 + \Lambda_y$ (denoted by the thick solid line in Fig. 2). Because $-1 < \mathcal{G}_\alpha < 1$, it follows from Eq. (43) that the discontinuity of $\partial^2 S_\alpha / \partial l^2$ is due to the discontinuity of $\partial^2 \mathcal{G}_\alpha / \partial l^2$. Similarly, it can be shown that $\partial^2 S_\alpha / \partial l^2$ also exhibits a discontinuity on the critical lines $\Lambda_y = 1 + \Lambda_x$ and $\Lambda_x = 1 - \Lambda_y$ (denoted by the thick dashed and dotted lines in Fig. 2) which is due to the discontinuity of $\partial^2 \mathcal{G}_\alpha / \partial l^2$ on these lines. As in Fig. 3, we choose $\Lambda = 0.1$, $\varphi = 0$ and $\Lambda_y = 0.5$ as a typical example to show S_x and its first and second derivatives with respect to Λ_x (see Fig. 4). It is clear that S_x and its first derivative $\partial S_x / \partial \Lambda_x$ are continuous as a function of Λ_x , but its second derivative $\partial^2 S_x / \partial \Lambda_x^2$ is discontinuous at the quantum phase transition points $\Lambda_x = 0.5$ and $\Lambda_x = 1.5$.

As shown above, both the nonanalyticity of the ground-state energy and that of the bipartite entanglement are due to the nonanalyticity of the spin-spin correlation functions. This reveals that the ground-state energy and the bipartite entanglement are closely related with each other, and both of them can be used to characterize the topological quantum phase transition in the extended Kitaev spin model.

IV. CONCLUSION

In conclusion, we have studied the topological quantum phase transition between Abelian and non-Abelian phases in an extended Kitaev model on a honeycomb lattice. This extended Kitaev model differs from the Kitaev model used in Ref. [11] as follows: (i) The lattice is placed on a torus instead of a cylinder, and (ii) the Hamiltonian in the extended Kitaev model breaks time reversal symmetry. From the ground-state energy, we show that the extended Kitaev model displays a continuous quantum phase transition on the critical lines separating the Abelian and non-Abelian phases, where the third derivative of the ground-state energy is discontinuous. Also, we use the von Neumann entropy as a measure of bipartite entanglement to study the topological quantum phase transition. The results show that the bipartite entanglement is also nonanalytic on the same critical lines as the ground-state energy. Moreover, we show that the discontinuity of the second derivative of

the bipartite entanglement is related to the discontinuity of the third derivative of the ground-state energy. Our approach directly reveals that both the entanglement and the ground-state energy can be used to characterize the topological quantum phase transition in the extended Kitaev model.

Acknowledgments

We thank Z.D. Wang and Yan Chen for useful discussions. This work was supported in part by the National Security Agency, the Laboratory for Physical Sciences, the Army Research Office, and the National Science Foundation Grant No. EIA-0130383. J.Q.Y. and X.F.S. were also supported by the National Basic Research Program of China grant Nos. 2009CB929300 and 2006CB921205, the National Natural Science Foundation of China grant Nos. 10625416, and the MOST grant No. 2008DFA01930.

APPENDIX A

This appendix focuses on the analyticity of the first, second and third directional derivatives of the ground-state energy on the critical line denoted by the thick solid line in Fig. 2. From Eq. (15), the derivative of the ground-state energy with respect to Λ_x is

$$\begin{aligned} \frac{\partial E}{\partial \Lambda_x} &= -\frac{\sqrt{3}}{16\pi^2} \int_{\text{BZ}} d^2k \frac{\partial}{\partial \Lambda_x} \varepsilon(\mathbf{k}) \\ &= -\frac{\sqrt{3}}{16\pi^2} \int_{\text{BZ}} d^2k \frac{A}{\varepsilon(\mathbf{k})} \\ &= -\frac{\sqrt{3}}{16\pi^2} \int_{\text{D}} d^2k \frac{A}{\varepsilon(\mathbf{k})} - \frac{\sqrt{3}}{16\pi^2} \int_{\text{BZ-D}} d^2k \frac{A}{\varepsilon(\mathbf{k})}, \end{aligned} \quad (A1)$$

where

$$A = \Lambda_x + \Lambda_y \cos k_x - \cos \left(\frac{k_x + \sqrt{3}k_y}{2} \right), \quad (A2)$$

and D denotes two small regions in the first Brillouin zone, i.e., half of the disk with radius ϵ , which is centered at $(\pi, -\pi/\sqrt{3})$, and half of the disk with radius ϵ , which is centered at $(-\pi, \pi/\sqrt{3})$, where $\epsilon \ll 1$. When $\Lambda_x - \Lambda_y = 1$, $\varepsilon(\mathbf{k})$ becomes zero only at the points $(\mp\pi, \pm\pi/\sqrt{3})$, so $\int_{\text{BZ-D}} d^2k \frac{A}{\varepsilon(\mathbf{k})}$ is analytic because BZ - D is the region excluding D in the first Brillouin zone. For the integral in the region D, we can approximate it as

$$\begin{aligned} \int_{\text{D}} d^2k \frac{A}{\varepsilon(\mathbf{k})} &\simeq \int_0^{2\pi} d\theta \int_0^\epsilon K dK \frac{\Delta + K^2 S_1}{\sqrt{\Delta^2 + K^2 S_2}} \\ &= \int_0^{2\pi} d\theta \left[\sqrt{\Delta^2 + \epsilon^2 S_2} - |\Delta| \right] \frac{\Delta}{S_2} \end{aligned}$$

$$\begin{aligned}
& + \int_0^{2\pi} d\theta \left[\frac{1}{3} (\Delta^2 + \epsilon^2 S_2)^{\frac{3}{2}} - |\Delta|^3 \right] \frac{S_1}{S_2^2} \\
& - \int_0^{2\pi} d\theta \frac{S_1 \Delta^2 \sqrt{\Delta^2 + \epsilon^2 S_2}}{S_2^2} \\
& + \int_0^{2\pi} d\theta |\Delta|^3 \frac{S_1}{S_2^2}, \tag{A3}
\end{aligned}$$

where

$$\begin{aligned}
\Delta &= \Lambda_x - \Lambda_y - 1, \\
S_1 &= P_1 + P_2 \sin(2\theta + \phi_2), \\
S_2 &= Q_1 + Q_2 \sin(2\theta + \phi_1), \tag{A4}
\end{aligned}$$

and

$$\begin{aligned}
Q_1 &= \frac{\Lambda_x \Lambda_y + 4\Lambda^2 + \Lambda_x - \Lambda_y}{2}, \\
Q_2 &= \frac{1}{4} \sqrt{(2\Lambda_x \Lambda_y + 8\Lambda^2 - \Lambda_x + \Lambda_y)^2 + 3(\Lambda_x + \Lambda_y)^2}, \\
P_1 &= \frac{\Lambda_y + 1}{4}, \\
P_2 &= \frac{1}{4} \sqrt{\Lambda_y^2 - \Lambda_y + 1}, \\
\phi_1 &= \arctan \left(\frac{2\Lambda_x \Lambda_y + 8\Lambda^2 - \Lambda_x + \Lambda_y}{\sqrt{3}(\Lambda_x + \Lambda_y)} \right), \\
\phi_2 &= \arctan \left(\frac{2\Lambda_y - 1}{\sqrt{3}} \right). \tag{A5}
\end{aligned}$$

From Eq. (A3), we have

$$\begin{aligned}
\int_D d^2k \frac{A}{\epsilon(\mathbf{k})} \Big|_{1+} &\simeq \frac{\epsilon^3}{3} \int_0^{2\pi} d\theta \frac{S_1}{S_2^2}, \\
\int_D d^2k \frac{A}{\epsilon(\mathbf{k})} \Big|_{1-} &\simeq \frac{\epsilon^3}{3} \int_0^{2\pi} d\theta \frac{S_1}{S_2^2}, \tag{A6}
\end{aligned}$$

where 1^+ denotes $\Lambda_x - \Lambda_y \rightarrow 1$ with $\Lambda_x - \Lambda_y > 1$, and 1^- denotes $\Lambda_x - \Lambda_y \rightarrow 1$ with $\Lambda_x - \Lambda_y < 1$. When $\epsilon \rightarrow 0$, it follows from Eq. (A6) that $\int_{\text{BZ-D}} d^2k \frac{A}{\epsilon(\mathbf{k})} \rightarrow 0$ on the critical line $\Lambda_x = 1 + \Lambda_y$ (i.e., the thick solid line in Fig. 2). Thus, from Eq. (A1), we have

$$\frac{\partial E}{\partial \Lambda_x} \Big|_{1+} = \frac{\partial E}{\partial \Lambda_x} \Big|_{1-}. \tag{A7}$$

Similarly,

$$\frac{\partial E}{\partial \Lambda_y} \Big|_{1+} = \frac{\partial E}{\partial \Lambda_y} \Big|_{1-}. \tag{A8}$$

From Eqs. (16), (A7), and (A8), it follows that

$$\frac{\partial E}{\partial l} \Big|_{1+} = \frac{\partial E}{\partial l} \Big|_{1-}. \tag{A9}$$

Using the same procedure as above, we can obtain

$$\begin{aligned}
\frac{\partial^2 E}{\partial l^2} \Big|_{1+} &= \frac{\partial^2 E}{\partial l^2} \Big|_{1-}, \\
\frac{\partial^3 E}{\partial l^3} \Big|_{1+} - \frac{\partial^3 E}{\partial l^3} \Big|_{1-} &\simeq \frac{\sqrt{3}\Gamma}{4\pi^2} (\cos \varphi - \sin \varphi)^3, \tag{A10}
\end{aligned}$$

where

$$\Gamma \equiv \int_0^{2\pi} d\theta \frac{1}{Q_1 + Q_2 \sin(2\theta + \phi_1)}. \tag{A11}$$

APPENDIX B

This appendix gives results regarding the analyticity of the correlation function \mathcal{G}_α ($\alpha = x, y$) and its first, and second directional derivatives on the critical line denoted by the thick solid line in Fig. 2. Similar to Eq. (A1), one can divide the integral in (32) into two parts:

$$\begin{aligned}
\mathcal{G}_x &= -\frac{\sqrt{3}}{8\pi^2} \int_{\text{BZ}} d^2k \frac{A}{\epsilon(\mathbf{k})} \\
&= -\frac{\sqrt{3}}{8\pi^2} \int_D d^2k \frac{A}{\epsilon(\mathbf{k})} - \frac{\sqrt{3}}{8\pi^2} \int_{\text{BZ-D}} d^2k \frac{A}{\epsilon(\mathbf{k})}, \tag{B1}
\end{aligned}$$

where A is given in Eq. (A2). Using the same procedure for Eqs. (A9) and (A10), we can derive from Eq. (B1) that

$$\mathcal{G}_x|_{1+} = \mathcal{G}_x|_{1-}, \tag{B2}$$

and

$$\begin{aligned}
\frac{\partial \mathcal{G}_x}{\partial \Lambda_x} \Big|_{1+} &= \frac{\partial \mathcal{G}_x}{\partial \Lambda_x} \Big|_{1-}, \\
\frac{\partial \mathcal{G}_x}{\partial \Lambda_y} \Big|_{1+} &= \frac{\partial \mathcal{G}_x}{\partial \Lambda_y} \Big|_{1-}, \\
\frac{\partial^2 \mathcal{G}_x}{\partial \Lambda_x^2} \Big|_{1+} - \frac{\partial^2 \mathcal{G}_x}{\partial \Lambda_x^2} \Big|_{1-} &\simeq \frac{\sqrt{3}}{2\pi^2} \Gamma, \\
\frac{\partial^2 \mathcal{G}_x}{\partial \Lambda_x \partial \Lambda_y} \Big|_{1+} - \frac{\partial^2 \mathcal{G}_x}{\partial \Lambda_x \partial \Lambda_y} \Big|_{1-} &\simeq -\frac{\sqrt{3}}{2\pi^2} \Gamma, \\
\frac{\partial^2 \mathcal{G}_x}{\partial \Lambda_y^2} \Big|_{1+} - \frac{\partial^2 \mathcal{G}_x}{\partial \Lambda_y^2} \Big|_{1-} &\simeq \frac{\sqrt{3}}{2\pi^2} \Gamma, \tag{B3}
\end{aligned}$$

where Γ is given in Eq. (A11).

From Eq. (34), we can obtain

$$\begin{aligned}
\mathcal{G}_y|_{1+} &= \mathcal{G}_y|_{1-}, \\
\frac{\partial \mathcal{G}_y}{\partial \Lambda_x} \Big|_{1+} &= \frac{\partial \mathcal{G}_y}{\partial \Lambda_x} \Big|_{1-}, \\
\frac{\partial \mathcal{G}_y}{\partial \Lambda_y} \Big|_{1+} &= \frac{\partial \mathcal{G}_y}{\partial \Lambda_y} \Big|_{1-}, \\
\frac{\partial^2 \mathcal{G}_y}{\partial \Lambda_x^2} \Big|_{1+} - \frac{\partial^2 \mathcal{G}_y}{\partial \Lambda_x^2} \Big|_{1-} &\simeq -\frac{\sqrt{3}}{2\pi^2} \Gamma, \\
\frac{\partial^2 \mathcal{G}_y}{\partial \Lambda_x \partial \Lambda_y} \Big|_{1+} - \frac{\partial^2 \mathcal{G}_y}{\partial \Lambda_x \partial \Lambda_y} \Big|_{1-} &\simeq \frac{\sqrt{3}}{2\pi^2} \Gamma, \\
\frac{\partial^2 \mathcal{G}_y}{\partial \Lambda_y^2} \Big|_{1+} - \frac{\partial^2 \mathcal{G}_y}{\partial \Lambda_y^2} \Big|_{1-} &\simeq -\frac{\sqrt{3}}{2\pi^2} \Gamma. \tag{B4}
\end{aligned}$$

-
- [1] S. L. Sondhi, S. M. Girvin, J. P. Carini, and D. Shahar, Rev. Mod. Phys. **69**, 315 (1997).
 - [2] S. Sachdev, *Quantum Phase Transitions* (Cambridge University Press, Cambridge, 1999).
 - [3] X. G. Wen and Q. Niu, Phys. Rev. B **41**, 9377 (1990).
 - [4] X. G. Wen, *Quantum Field Theory of Many-Body Systems* (Oxford University, Oxford, 2004).
 - [5] D. Arovas, J. R. Schrieffer, and F. Wilczek, Phys. Rev. Lett. **53**, 722 (1984).
 - [6] F. D. M. Haldane and E. H. Rezayi, Phys. Rev. B **31**, 2529 (1985).
 - [7] A. Kitaev and J. Preskill, Phys. Rev. Lett. **96**, 110404 (2006).
 - [8] M. Levin and X. G. Wen, Phys. Rev. Lett. **96**, 110405 (2006).
 - [9] A. Kitaev, Ann. Phys. (N. Y.) **321**, 2 (2006).
 - [10] D. H. Lee, G. M. Zhang, and T. Xiang, Phys. Rev. Lett. **99**, 196805 (2007).
 - [11] X. Y. Feng, G. M. Zhang, and T. Xiang, Phys. Rev. Lett. **98**, 087204 (2007).
 - [12] S. Mondal, D. Sen, and K. Sengupta, Phys. Rev. B **78**, 045101 (2008).
 - [13] E. Lieb, T. Schultz, and D. Mattis, Ann. Phys. (N. Y.) **60**, 407 (1961).
 - [14] E. H. Lieb, Phys. Rev. Lett. **73**, 2158 (1994).
 - [15] S. Yang, S. J. Gu, C. P. Sun and H. Q. Lin, Phys. Rev. A **78**, 012304 (2008).
 - [16] T. J. Osborne and M. A. Nielsen, Phys. Rev. A **66**, 032110 (2002).
 - [17] A. Osterloh *et al.* Nature **416**, 608 (2002).
 - [18] G. Vidal, J. I. Latorre, E. Rico, and A. Kitaev, Phys. Rev. Lett. **90**, 227902 (2003).
 - [19] Y. Chen, Z. D. Wang, and F. C. Zhang, Phys. Rev. A **73**, 224414 (2006).
 - [20] S. J. Gu, S. H. Deng, Y. Q. Li, and H. Q. Lin, Phys. Rev. Lett. **93**, 086402 (2004).
 - [21] L. A. Wu, M. S. Sarandy, and D. A. Lidar, Phys. Rev. Lett. **93**, 250404 (2004).
 - [22] L. A. Wu, M. S. Sarandy, D. A. Lidar, and L. J. Sham, Phys. Rev. A **74**, 052335 (2006).
 - [23] R. P. Feynman, Phys. Rev. **56**, 340 (1935).
 - [24] M. A. Nielsen and I. L. Chuang, *Quantum Computation and Quantum Information* (Cambridge University Press, Cambridge, 2000).
 - [25] X. G. Wang and P. Zanardi, Phys. Lett. A **301**, 1 (2002).